Spark Ablation: a dry, physical, and continuous method to prepare powdery metal nanoparticle-based catalysts

Damien P. Debecker,[1,*] Plaifa Hongmanorom,[1] Tobias V. Pfeiffer,[2] Bernardus Zijlstra,[2] Yingrui Zhao,[1] Sandra Casale,[3] Capucine Sassoye[4]

[1] Institute of Condensed Matter and Nanoscience (IMCN), UCLouvain, 1348 Louvain-La-Neuve, Belgium

[2] VSParticle B.V., Oostsingel 209, 2612HL, Delft, the Netherlands.

[3] Laboratoire de Réactivité de Surface (LRS), Sorbonne Université, UMR 7197 CNRS, 4 Place Jussieu, 75005, Paris, France

[4] Laboratoire de Chimie de la Matière Condensée de Paris (LCMCP), Sorbonne université, UMR 7574 CNRS -Sorbonne Université, Campus Pierre et Marie Curie, 4 Place Jussieu, F-75005 Paris, (France)

* Corresponding Author: damien.debecker@uclouvain.be

Experimental

Catalyst synthesis

To obtain optimal dispersion of fine Ni clusters throughout the nanostructured TiO_2 support particles, a gas phase approach was taken. Two separate aerosols are generated and subsequently mixed. As the particles coagulate, bigger particles scavenge smaller particles, resulting in preferential coating ("decorating") of the TiO_2 support particles with Nickel clusters.[1] To achieve this, a new setup was developed to ensure the two aerosols are finely dispersed and mixed at consistent rates.

An overview of the schematic is presented in Fig. S1 below. A powder reservoir is partially filled with the support material. Powder is dispensed from this reservoir, subsequently de-agglomerated by shear in a venturi nozzle. The powder is then injected into the spark generator, where the metal clusters are generated by spark ablation. The mixed aerosol is finally collected onto a filter disc.

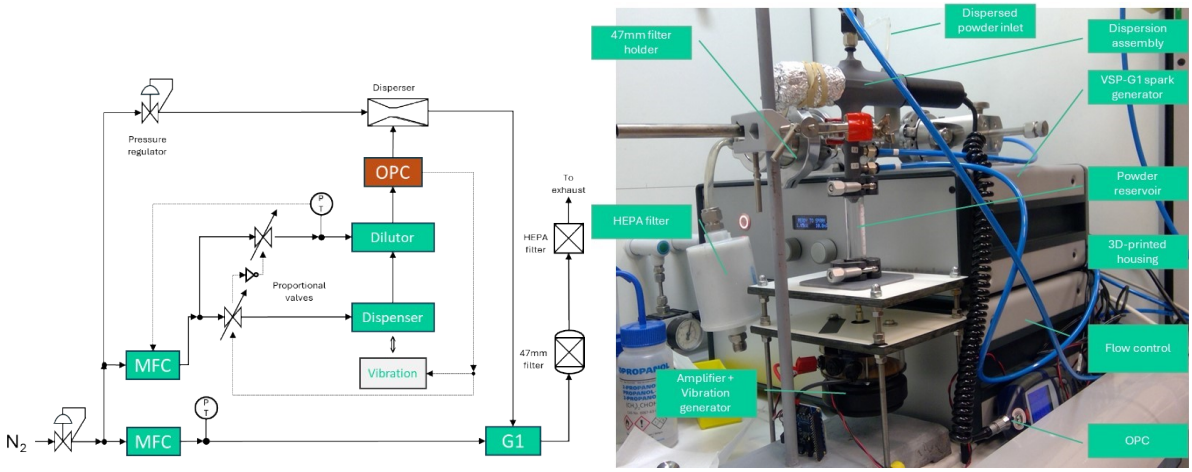

Fig. S1 (Left) Process schematic and (Right) Photograph of the dispersion assembly.

Spark ablation generator

The Ni particles were generated in the VSP-G1 Nanoparticle Generator (VSP-G1, VSParticle, the Netherlands) via spark ablation from nickel electrodes (3mm diameter; 99.99% purity). N_2 (99.9% purity; 3.0 slpm) was used as an inert carrier gas and the G1 was operated at 1.3 kV and 10.4 mA as a gap voltage and charging current, respectively. All flows were controlled by mass flow controllers (Bronkhorst, the Netherlands).

A short residence time after the spark limits agglomeration, and ensures the generated particles are collected as small clusters onto the powder.[1] The reactor chamber of the G1 was modified with an extra inlet and an insert that injects a stream of aerosolized powder just downstream of the spark (Fig. S2).

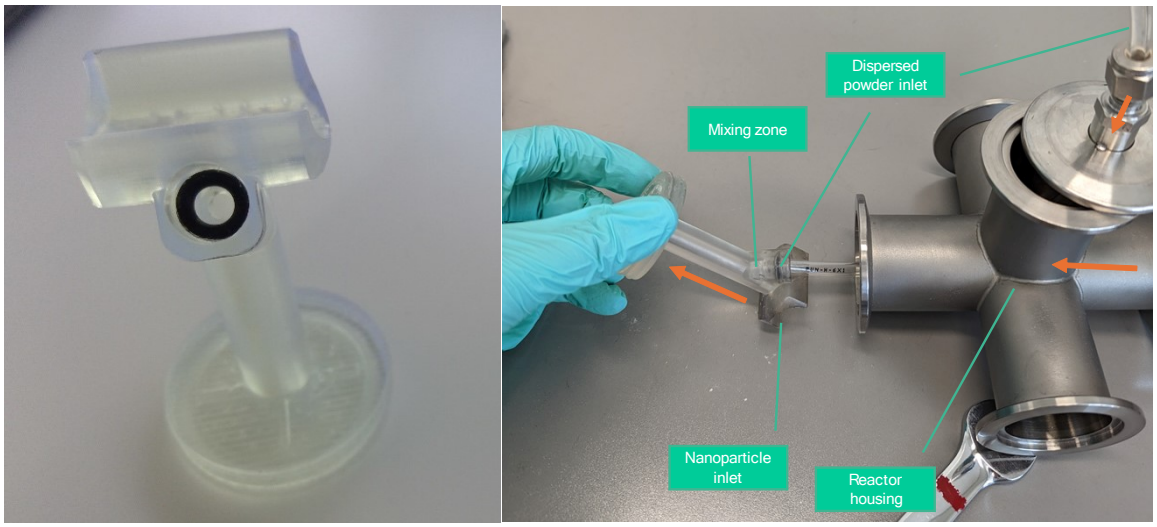

Fig. S2 (Left) Mixing insert and (Right) Assembling the mixing insert in the spark generator reactor housing.

Powder disperser

The carrier powder, TiO_2 P25 (Degussa), was aerosolized from a vibrating reservoir by a jet of N_2 gas (Fig. S1 (Left), Fig. S3). The reservoir comprised a glass tube with KF flanges, with a thin sheet of nitrile rubber stretched across the bottom. The rubber base is agitated by the vibration generator (VOS-40042, VOS instrumenten, the Netherlands). The aerosol concentration can be controlled in two ways: by changing the vibration frequency and intensity, and by changing the ratio of carrier gas flow (2.8 slpm in total) distributed between the dispenser and a dilution stage (Fig. S3 (Right)). Powder concentration was monitored with an optical particle counter (OPC) (Microdust Pro, Casella, UK), modified to ensure the system is leak tight ($<10^{-4}$ mbar.L.s^{-1}). The aerosolized particles were subsequently deagglomerated in a venturi vacuum generator (AVRG038H, Air-Vac, USA, inlet pressure 2.5 bar) before being introduced into the G1 spark generator.[2, 3] Afterwards, the mixed aerosol was collected on a 0.65µm pore-size, hydrophylic PVDF filter (DVPP04700, Merck Millipore), as a light-grey powder.

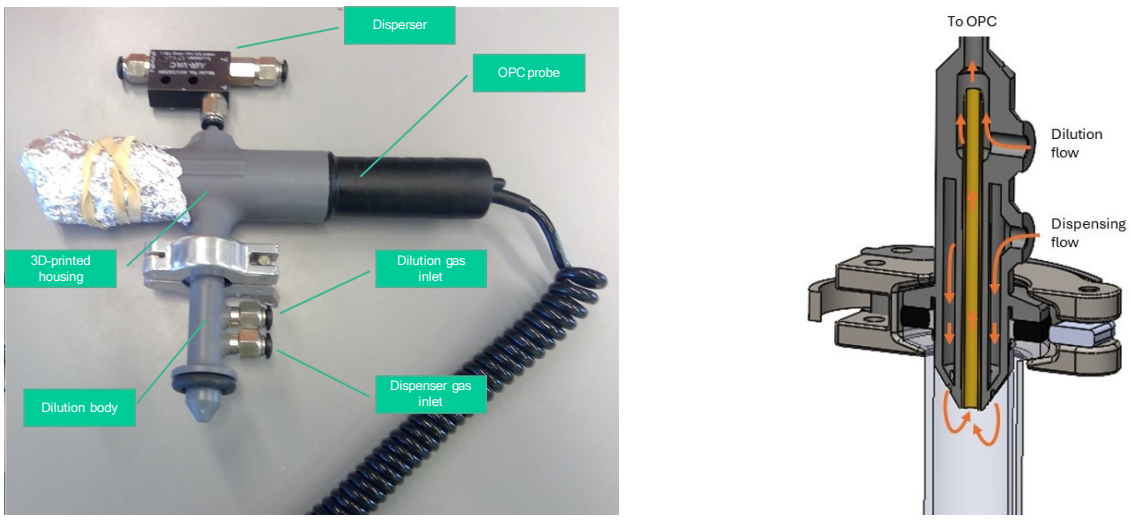

Fig. S3 (Left) Photo of the disperser assembly and (Right) Detailed view of the dispenser/dilution module.

Characterization

Textural properties were determined from N_2 physisorption isotherms carried out at -196 °C on a Tristar 3000 instrument from Micrometrics. Prior to the analysis, the sample was degassed under vacuum at 200 °C overnight to eliminate the physically adsorbed water and other volatile species. The specific surface area was evaluated by the Brunauer-Emmett-Teller (BET) method in the relative pressure (P/P_0) range of 0.05-0.3. The total pore volume was measured from the adsorption branch at $P/P_0 \sim 0.98$, and the average pore diameter was estimated from the adsorption isotherm using Barrett-Joyner-Halenda (BJH) method.

H_2-temperature programmed reduction (H_2-TPR) experiment was conducted using a BELCAT II, Microtrac. Approximately 40 mg of catalyst was initially outgassed under Ar flow of 50 mL/min at 200 °C to remove physisorbed water and impurities. After cooling down to 100 °C, the H_2-TPR profile was then obtained over a temperature from 100 °C to 500 °C, with a heating rate of 10 °C/min, under 50 mL/min of 1% (v/v) H_2 diluted in Ar.

The crystallinity and phase identification were investigated by a Bruker AXS-D8 Advance diffractometer using Cu Kα (λ = 1.54 Å) radiation at 35 kV and 40 mA.

The weight percentage of Ni in the catalyst was measured by inductively coupled plasma atomic emission spectroscopy (ICP-AES) on an ICAP 6500 instrument from Thermo Scientific. The sample was dissolved by sodium peroxide fusion before the measurement.

High Resolution Transmission electron microscopy (TEM) was performed using JEOL-Plus (LaB6) equipped with an Oxford EDX detector.

CO_2 methanation

The catalytic performance was evaluated in a continuous flow fixed-bed reactor under atmospheric pressure. 200 mg of catalyst was loaded into the reactor and reduced in situ at 500 °C for 2 h under 20 mL/min of 50% H_2/50% He. After purging with He and cooling down to 200 °C, a reaction mixture of 10% CO_2 and 40% H_2 diluted in He (total flow rate of 20 mL/min) was fed to the reactor. The catalytic test was performed in a temperature range of 200–400 °C, and each temperature was maintained for 88 min to allow four gas chromatograph injections. The outlet gases were quantified by a gas chromatograph (Varian CP3800) equipped with Hayesep Q, Molsieve 5A, and CP-Sil-5CB columns. The separated CO and CO_2 were analyzed by a thermal conductivity detector, while CH_4 was detected with a flame ionization detector. All gas transfer lines were heated at 125 °C to prevent the condensation of water by-product. The CO_2 conversion (X_{CO_2}), CH_4 selectivity (S_{CH_4}) and CO_2 conversion rate ($mol \cdot g_{Ni}^{-1} \cdot h^{-1}$) were calculated according to the following equations, in which F, m_{cat} and ω_{Ni} are the molar flow rate, mass of catalyst and Ni loading, respectively:

$$X_{CO_2} = \frac{F_{CO_{2,in}} - F_{CO_{2,out}}}{F_{CO_{2,in}}} \times 100\%$$

$$S_{CH_4} = \frac{F_{CH_{4,out}}}{F_{CO_{2,in}} - F_{CO_{2,out}}} \times 100\%$$

$$CO_2\ conversion\ rate = \frac{X_{CO_2} \times F_{CO_{2,in}}}{m_{cat} \times \omega_{Ni}} \times 100\%$$

Additional data

Table S1. Comparison of CO_2 conversion rates on the reported Ni catalysts in CO_2 methanation at 300 °C.

Catalyst	Preparation method	WHSV ($mL \cdot g_{cat}^{-1} \cdot h^{-1}$)	CO_2 conversion (%) [a]	CH_4 selectivity (%) [a]	CO_2 conversion rate ($mol \cdot g_{Ni}^{-1} \cdot h^{-1}$)	Ref.
2.3%Ni/TiO_2	Spark-ablation	6000	10.1	71.6	0.12	This work
12%Ni/TiO_2	Sol-gel	48,000	3.0	97.0	0.08	[4]
5.7%Ni/CeO_2	Citrate sol-gel	10,000	20	95.0	0.13	[5]
20%Ni/Al_2O_3	Microwave	4200	88.0	99.3	0.09	[6]
14.89%Ni/Al_2O_3	Impregnation	30,000	9.0	96.0	0.16	[7]
10%Ni/Al_2O_3	Evaporation induced self-assembly	30,000	9.0	87.5	0.18	[8]
50%Ni/SiO_2	Sol-gel	24,000	78.0	95.0	0.17	[9]
20%Ni/Al_2O_3-ZrO_2	Epoxide-driven sol-gel	6000	77	99.0	0.21	[10]
10%Ni@MOF-5	Impregnation	7,500	75.1	100.0	0.30	[11]
5.7%Ni/CeO_2-g-C_3N_4	Citrate sol-gel	10,000	48	99.0	0.30	[5]
10%Ni/Zr-TiO_2	Sol-gel	48,000	15	98.0	0.48	[12]

[a] CO_2 conversion and CH_4 selectivity values were obtained from figure or table.

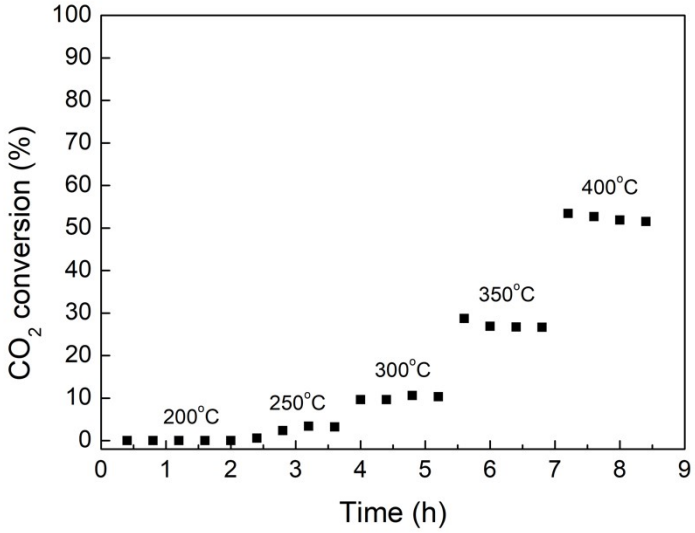

Fig. S4 CO_2 conversion of the Ni/TiO_2 catalyst as a function of time (data reported in Fig. 4 are averages of the data points reported here for each temperature).

The catalyst is fully stable when tested at moderate temperature (200°C – 300°C). At high temperatures of 350 °C and 400 °C, however, a slow decrease in CO_2 conversion could be observed. It is widely recognized that elevated reaction temperatures, coupled with the exothermic nature of CO_2 methanation, can lead to the sintering of Ni nanoparticles, causing catalyst deactivation and loss of catalytic performance.[15, 16] It is likely that large Ni nanoparticles formed from the sintering of "floating" Ni nanoparticles without interaction with TiO_2 may result in progressively lowering CO_2 conversion due to a decreased active metal surface area for CO_2 and H_2 activation.

Additional discussion

The effect of metal-support interaction

It has been reported that the classical strong metal-support interaction (SMSI) effect can positively influence the geometry and electronic properties of the Ni/TiO_2 catalyst, thereby enhancing the adsorption and activation of CO_2 and H_2 or the adsorption of key intermediate species during CO_2 methanation.[12, 13]. However, the strong interaction between Ni and partially reducible TiO_2 can also lead to the formation of TiO_2 overlayer around Ni nanoparticles, which blocks catalytic active sites and hinders the reactant activation.[14] Therefore, the metal-support interaction in the Ni/TiO_2 catalyst needs to be tuned to achieve high CO_2 methanation activity. Here, TPR data clearly show the presence of at least two types of Ni particle (partially passivated to NiO) with different degrees of interaction with the support. Further optimization of the spark-preparation process should be aimed at suppressing the formation of aggregates of "floating" Ni particles that do not interact with the TiO_2 support and seem to sinter heavily, resulting in activity loss. For the small and dispersed particles, it is worthwhile to explore whether the metal-support interaction established via this "clean" preparation show similarities to those of catalysts prepared by classical methods in future studies.

References

1. T. V. Pfeiffer, P. Kedia, M. E. Messing, M. Valvo and A. Schmidt-Ott, *Materials*, 2015, **8**, 1027-1042.
2. L. Pokharel, P. Parajuli, L. Li, E. J. Chng and R. Gopalakrishnan, *Aerosol Sci. Technol.*, 2019, **53**, 321-331.
3. A. J. Tiwari, C. G. Fields and L. C. Marr, *Aerosol Sci. Technol.*, 2013, **47**, 1267-1275.
4. P. Unwiset, K. C. Chanapattharapol, P. Kidkhunthod, Y. Poo-arporn and B. Ohtani, *Chem. Eng. Sci.*, 2020, **228**, 115955.
5. Y. Yu, Y. M. Chan, Z. Bian, F. Song, J. Wang, Q. Zhong and S. Kawi, *Int. J. Hydrogen Energy*, 2018, **43**, 15191-15204.
6. F. Song, Q. Zhong, Y. Yu, M. Shi, Y. Wu, J. Hu and Y. Song, *Int. J. Hydrogen Energy*, 2017, **42**, 4174-4183.
7. L. Bian, L. Zhang, R. Xia and Z. Li, *Journal of Natural Gas Science and Engineering*, 2015, **27**, 1189-1194.
8. Q. Liu, S. Wang, G. Zhao, H. Yang, M. Yuan, X. An, H. Zhou, Y. Qiao and Y. Tian, *Int. J. Hydrogen Energy*, 2018, **43**, 239-250.
9. Y. Zhao, V. Girelli, O. Ersen and D. P. Debecker, *J. Catal.*, 2023, **426**, 283-293.
10. J. Lin, C. Ma, Q. Wang, Y. Xu, G. Ma, J. Wang, H. Wang, C. Dong, C. Zhang and M. Ding, *Appl. Catal., B*, 2019, **243**, 262-272.
11. W. Zhen, B. Li, G. Lu and J. Ma, *Chem. Commun.*, 2015, **51**, 1728-1731.
12. A. Makdee, P. Kidkhunthod, Y. Poo-arporn and K. C. Chanapattharapol, *Journal of Environmental Chemical Engineering*, 2022, **10**, 107710.
13. J. Ma, T. Liu, G. Chen, S. Liu, W. Gong, Y. Bai, H. Liu, Y. Wang, D. Liu, R. Long, Y. Li and Y. Xiong, *Applied Catalysis B: Environment and Energy*, 2024, **344**, 123600.
14. J. Li, Y. Lin, X. Pan, D. Miao, D. Ding, Y. Cui, J. Dong and X. Bao, *ACS Catal.*, 2019, **9**, 6342-6348.
15. P. Hongmanorom, J. Ashok, G. Zhang, Z. Bian, M. H. Wai, Y. Zeng, S. Xi, A. Borgna and S. Kawi, *Appl. Catal., B*, 2021, **282**, 119564.
16. B. Miao, S. S. K. Ma, X. Wang, H. Su and S. H. Chan, *Catal. Sci. Technol.*, 2016, **6**, 4048-4058.